Title
TOMOGRAPHIC IMAGE RECONSTRUCTION BY EIGENVECTOR DECOMPOSITION: ITS LIMITATIONS AND AREAS OF APPLICABILITY

Author
Llacer, J.

Publication Date
1982

LBL-13573
Preprint

Lawrence Berkeley Laboratory
UNIVERSITY OF CALIFORNIA

Engineering & Technical
Services Division

To be published in IEEE Transactions in Medical Imaging

TOMOGRAPHIC IMAGE RECONSTRUCTION BY EIGENVECTOR DECOMPOSITION: ITS LIMITATIONS AND AREAS OF APPLICABILITY

Jorge Llacer

January 1982

Prepared for the U.S. Department of Energy under Contract W-7405-ENG-48

DISCLAIMER

LBL-13573

TOMOGRAPHIC IMAGE RECONSTRUCTION BY EIGENVECTOR DECOMPOSITION: ITS LIMITATIONS AND AREAS OF APPLICABILITY*

Jorge Llacer
Lawrence Berkeley Laboratory
University of California
Berkeley, California 94720, U.S.A.

Abstract

This paper analyzes in detail the process of tomographic image reconstruction by pseudo-inversion of the blurring matrix of a PET imaging system. Eigenvector and eigenvalue decomposition is used as a method to evaluate the physical reasons for the ill-conditioned nature of the problem. It is shown that finding an accurate pseudo-inverse for even a modest PET array of 8 x 8 pixels is a difficult task for a computer with 48-bit mantissa. The problem is caused by the strong ambiguity with which the detector system measures the activity at each pixel.

For a problem in which imaging with a complete detector ring is not possible, and in which invariance of the point response function cannot be maintained, the pseudo-inverse method of reconstruction is, however, shown to be very useful. Advantage is taken of the fact that the activity to be measured is localized in a single plane, without over or underlying activity. A planar camera configuration yields very well conditioned matrices that are separable for a large number of useful cases. It is even possible to define pixel sizes which are considerably smaller than the detector size and solve the problem without a substantial increase in the noise magnification factor.

Recognizing that the above application is equivalent to a case of very well defined time-of-flight (TOF) measurement, the simple initial PET study is

*This paper was prepared under the auspices of the U.S. Dept. of Energy Contract W-7405-ENG-48 and a grant from the National Institute of Health No. CA27024-02. The figures were printed from originals provided by the author.

reevaluated by inclusion of TOF information. It is shown that even with TOF uncertainty of the order of several pixels in size, the condition of the problem improves greatly, with decrease of one order of magnitude in noise propagation.

Introduction

Tomographic image reconstruction by the filtered backprojection technique has become the almost universal image reconstruction method both in computerized X-ray tomography (CAT) and in single photon or positron emission tomography (SPET, PET). In all cases, data from a complete set of views is required and the assumption that the point response function of the imaging system is space invariant must hold to a considerable extent. In contraposition, the idea of solving the imaging problem by inversion (or pseudo-inversion) of the matrix defining the imaging system has frequently been rejected in the literature due to the apparent need to invert or find the eigenvalues and eigenvectors of a matrix of dimensions $n^2 \times n^2$ for an image plane of dimensions n x n. For medical tomographic imaging, such matrices are badly behaved and the method seems to offer no hope.

At the Lawrence Berkeley Laboratory, we are examining an imaging problem in PET in which the existence of a complete ring of detectors is physically impossible and the limiting of the radiation acceptance cone in order to preserve space invariance is not acceptable because of the reduction in sensitivity that it entails. The problem arises in the process of injecting a beam of accelerated positron emitting nuclei into a patient and measuring the end point of the beam trajectory by imaging the annihilation gamma-rays emitted by the nuclei when they come to rest.[1] By that process, cancer radiation therapy

of small tumors localized in inoperable areas of the body can be aided by determining with great accuracy where the therapy heavy ions will deposit most of their cell killing energy, sparing healthy, sensitive structures in the patient.

The injection of a beam of positron emitting accelerated heavy ions would result in a heavy radiation dose to the patient if millicures of positron emitting activity were to result from the injection. For probing purposes, a dose of a few rads is the maximum that appears acceptable and, with heavy ions, the resulting injected activity is of the order of 0.1 or 0.2 microcuries, a very small amount. On the other hand, we have the advantage that we want to image a line or a plane of radioactivity without any other substantial underlying or overlying activity during the imaging time of a few seconds.

The above requirements have directed us to reexamine image reconstruction methods based on linear matrix analysis as a basis on which to build appropriate imaging instruments. A simple theoretical development for imaging along a line, with a description of the physical meaning of the system matrix, its eigenvalues and eigenvectors was published earlier[2], as an aid to designing a one-dimensional imaging instrument.[3] Although in a different context, that theoretical material is similar to the pseudo-inverse method of image analysis used quite frequently in fields other than medical tomography. Reference 4 provides a very complete and lucid exposition of imaging theory based on matrix analysis.

This paper shows the outcome of an investigation into the "pseudo-inverse" method of image reconstruction for arrays of increasing number of pixels in a plane. In particular, using as an example a single plane PET imaging problem of the simplest kind, the paper describes the generation of "backprojection" system matrices and the corresponding two-dimensional "blurring" matrices. A

physical interpretation of the eigenvectors and eigenvalues follows, as well as a discussion of the errors and difficulties that occur as the size of the pixel array increases beyond the very modest size of 8 x 8. The reasons for the very unfavorable "condition number" of the blurring matrices are explored, leading the way towards a more favorable configuration of detectors for the beam injection problem at hand. It is shown that a planar configuration for the imaging instrument, i.e., two multicrystal flat arrays of detectors, equidistant from the plane of positron beam injection, results in blurring matrices of favorable condition numbers which allow not only an image reconstruction without maintaining space invariance of the point response function, but also allows the "deconvolving" of the effects of detector response overlap when the pixels are nearly a factor of two smaller in size than the size of the detectors. Furthermore, it is shown that for the planar camera the resulting blurring matrices with regular arrays of detectors are exactly separable into Dirac products of two n x n matrices, making the eigenanalysis, "pseudo-inverse" determination and filtering processes much easier than in cases where $n^2 \times n^2$ matrices have to be handled.

Finally, after realizing that the advantage of the proposed geometry for the application on hand is derived from the implied knowledge of the plane of emission of the gamma rays, the effect of time-of-flight (TOF) information on the matrix characteristics of the simple PET geometry is analyzed and the beneficial noise-reducing effects of TOF information is demonstrated.

The System Matrix

Reference 2 discusses the system matrix A for general imaging systems and the solution of the image reconstruction problem in terms of the eigenvectors

and eigenvalues of the symmetric matrix resulting from the product A^TA, where A^T indicates the transpose of A. In this paper a specific simple PET imaging problem will be used in order to provide a familiar basis for a physical description of the mathematical results. In particular an imaging system consisting of two rows of perfect detectors that can rotate by an angle θ about the center of an n x n array of pixels will be considered, as shown in Fig. 1. The linear dimension d of the pixels and of the detectors will be taken to be equal, the pixels will be taken to be of uniform activity and, for a given angle θ, the response of detectors a and b in coincidence will be proportional to the area of p intersected by the field of view of the two detectors (shaded zone in p). Coincidences will only be allowed between detectors which are facing each other directly so that there can be N_c coincidences at each position θ.

The system matrix A is obtained by assuming that a unit activity is placed in pixel No. 1, the detectors are made to step in N_θ angles from $\theta \leq 0 < 180^\circ$ and the resulting coincidence rates (a total of $N_c \times N_\theta$) are recorded as the first column of matrix A. The unit activity is then placed in pixels Nos. 2, 3, ... to n^2, each time obtaining one column of A. The resulting matrix has $N_c \times N_\theta$ rows and n^2 columns.

In principle, the imaging problem consists in solving the equation:

$$A\vec{x} = \vec{k} \tag{1}$$

where $\vec{x}$ is an unknown vector of length n^2, corresponding to some activity distribution in the pixels and $\vec{k}$ is a vector of length $N_c \times N_\theta$ which is the result of a measurement. Thus, the A matrix contains all the information about the pixel-detector system necessary to solve the imaging problem.

The Blurring Matrix

The solution to Eq. (1) is equivalent to solving:

$$A^T A\vec{x} = A^T \vec{k} \tag{2}$$

where A^T is the transpose of A. We can then define $A' = A^T A$ and $\vec{k}' = A^T\vec{k}$ and rewrite Eq. (2) as:

$$A'\vec{x} = \vec{k}' \tag{3}$$

where A' is of dimension $n^2 \times n^2$, and $\vec{x}$ and $\vec{k}'$ are also of dimension n^2, the number of pixels. Matrix A' is symmetric and positive. The i^{th} row (or column) contains as elements the activity that the detector system would sense as existing in the i^{th} pixel when a source of unit strength is moved in succession from the first to the last pixel.[4] A contains, therefore, information of the "blurring" function for each pixel caused by the camera configuration. Figure 2 shows the blurring matrix obtained for the detector system of Fig. 1 for an 8 x 8 pixel array. The A' matrix is of dimension 64 x 64. Plotting each one of the columns of A' in a n x n array gives an image of the blurring suffered by each pixel when viewed by the detector system. This has been done for the first column of A' in the n = 8 case and it is shown in Fig. 3. For large n, the blurring function approaches the well known 1/r blurring function for a point source[5], for pixels not too close to the image array edges.

The Deblurring Matrix

The solution to Eq. (3) would be quite straightforward if the inverse of A' would be obtained for a practical imaging system. If we let $B = A'^{-1}$, then:

$$\vec{x} = B\,\vec{k}' \tag{4}$$

For this inverse to be obtainable successfully it is necessary that A' be well behaved. Further, for $\vec{x}$ to be a reasonable approximation to the correct activity distribution in the presence of statistical fluctuations, it is necessary that the condition number (CN = largest eigenvalue/smallest eigenvalue) of A' be relatively low. These two conditions are very closely related. Reference 2 shows in a rather intuitive approach that:

$$\vec{x} = \sum_i \frac{\alpha_i}{\lambda_i}\,\vec{\chi}_i \tag{5}$$

where λ_i are the eigenvalues of A', χ_i are the eigenvectors, and $\alpha_i = \langle \vec{\chi}_i, \vec{k}' \rangle$, dot products of the indicated vectors. If some λ_i's are much smaller than the rest, any statistical fluctuation reflected in the α_i value will result in large errors in the contribution to the final solution of the corresponding eigenvectors $\vec{\chi}_i$.

One way of obtaining a "pseudo-inverse" for A' consists in replacing α_i and $\vec{k}'$ Eq. (5) by their definitions, arriving at the expression

$$x_q = \sum_{i=1}^{n^2} \sum_{j=1}^{n^2} \sum_{p=1}^{N_c \times N_\theta} k_p\, a_{pj} \frac{\chi_i^j\, \chi_i^q}{\lambda_i} \tag{6}$$

where χ_i^j is the j^{th} element of the i^{th} eigenvector, a_{pj} are elements

of the rectangular system matrix A, and k_p are elements of the vector of coincidence rates obtained in a measurement.

If we consider first the summation over p, in Eq. (6), letting

$$h_j = \sum_{p=1}^{N_c \times N_\theta} k_p a_{pj}, \quad \text{for } 1 \leq j \leq n^2, \tag{7}$$

we realize that $\vec{h}$ is obtained by taking dot products of the vector obtained experimentally with columns of the system matrix A. This is a backprojection process of the experimental results using the prescription contained in A. Thus, the system matrix A is also a backprojection matrix and it will be designated with either name henceforth. We note that $\vec{h} = \vec{k}'$ in Eqs. (3) and (4).

In terms of the backprojected image $\vec{h}$, the final result is, therefore

$$x_q = \sum_{j=1}^{n^2} h_j b_{jq} \tag{8}$$

where b_{jq} is defined as

$$b_{jq} = \sum_{i=1}^{n^2} \frac{\chi^j_i \chi^q_i}{\lambda_i} \tag{9}$$

Equation (8) performs a "deblurring" operation on the backprojected experimental result and one would expect that the b_{jq} are the elements of the matrix B which is some approximation to A'^{-1}. Indeed, a more rigorous treatment of the problem (Ref. 4, Sec. 8.1) shows that the filter of Eq. (9) is the "pseudo-inverse" filter that yields the minimum least squares solution of minimum norm for the general image recovery problem with space variant response function.

Pseudo-inverses have been obtained for the simple PET system of Fig. 1 with n = 5, 8 and 13. For n = 5, the eigenvalue and eigenvector analysis was carried out with 23 and 55-bit mantissa floating point numbers using the older Jacobi method[6], with 27-bit mantissa by reduction to tridiagonal form by Householder's method and the QL algorithm[7], and with 48-bit mantissa by a similar method[8]. The results of the 55-bit Jacobi method and the two calculations by the QL algorithm yielded identical results up to the 6^{th} or 7^{th} decimal digit. The 23-bit mantissa Jacobi method had errors that resulted in noticeable discrepancies in simple image reconstruction tests. The condition number of the 25 x 25 A' matrix is shown in Table I. The number of angles N_θ was increased until the CN stablized at its lowest value.

For the n = 8 case, simple image reconstruction test from the "pseudo-inverse" obtained from eigenanalysis with the QL algorithm using 27-bit mantissa showed some slight but noticeable errors, shown below, which decreased somewhat when a 48-bit mantissa was used. The CN's obtained are shown in Table I.

For n = 13, the eigenanalysis with the QL algorithm using 27-bit mantissa yields a CN which is lower than that of the n = 8 case. A simple image reconstruction with the resulting pseudo-inverse shows substantial errors, indicating the unreliability of the obtained analysis. An attempt to use a 48-bit mantissa and QL algorithm results in serious convergence problems in the determination of the eigenvalues and for that reason the attempt was not continued.

Figures 4 a) through c) show the three eigenvectors with highest eigenvalues, and Figs. 4 d) through f) show the ones with smallest eigenvalues, for the n = 8 case. As seen from Eq. (5), the eigenvectors have the same dimensions as the pixel array and a weighted sum of them forms the final image.

The high eigenvalue vectors approximate two-dimensional sine and cosine products, although this resemblance with a Fourier basis is lost at the low eigenvalue vectors.

The deblurring matrices obtained for the three values of n studied have very similar characteristics to the one shown in Fig. 5 a), for n = 8. Removing some of the summation terms of Eq. (9) in forming matrix B changes its appearance quite drastically, as seen in Fig. 5 b). Leaving out some of the summation terms is a method of reducing noise in image restoration at the expense of sharpness. The effect on tomographic reconstruction will be discussed below.

Separability

As discussed in detail in Ref. 4, the problem of image restoration can be simplified greatly if the blurring matrix can be separated into the Dirac product of two blurring matrices X and Y, each of dimension n x n. In that case, the n^2 x n^2 matrix can be subdivided in such a way that the following description holds:

$$A = \begin{matrix} x_{11}Y & x_{12}Y \cdots x_{1n}Y \\ \vdots & \\ x_{n1}Y & x_{n2}Y \cdots x_{nn}Y \end{matrix} \qquad (10)$$

where x_{ij} are elements of the matrix X. If A can be subdivided in that way, filtering of the backprojected image can be carried out by

$$[x] = [B_x]\,[k']\,[B_y] \qquad (11)$$

where [x] and [k′] are the vectors $\vec{x}$ and $\vec{k}'$ represented as n x n matrices, and

$$[B_x] = [\chi_x]\,[\lambda_x^{-1}]\,[\chi_x]^T \qquad (12)$$

and similarly for $[B_y]$. Matrix $[\chi_x]$ is the n x n matrix of eigenvectors for the X blurring matrix and $[\lambda_x^{-1}]$ is a diagonal matrix containing the reciprocal of the corresponding eigenvalues.[4]

With separability it is only necessary to obtain pseudo-inverses for n x n matrices, instead of n^2 x n^2 for the general case. Unfortunately, the PET imaging problem of Fig. 1 is not separable. Separability would imply that blurring in the x-direction is only a function of x, and similarly for the y-direction. The blurring function $1/r = 1/\sqrt{x^2 + y^2}$ cannot be separated into a product $f(x) \cdot g(y)$ except in a crude manner that leads to very poor image reconstructions.

The saving simplification in the PET problem is in the assumption that the point response function becomes space invariant as n becomes large. In that case the eigenvectors of A form the Fourier basis and it allows for the successful development of the very useful imaging technology available today. Nevertheless, the problem remains a very badly posed one, requiring excellent statistics and absence of flaws in the raw image data for a good image.

Noise Magnification

An examination of Eq. (5) indicates that CN of an imaging system is not sufficient to define the noise magnification in a reconstruction. A large number of λ_i's may be involved in propagating statistical noise from individual projections to the final image as there may be a number of eigenvectors $\vec{\chi}_i$ that contain high frequency variations. It appears that the noise magnification factor would have to be calculated case by case for the non-Fourier based systems.

In order to gain some understanding of the noise magnification of the simple PET system described above for later comparison with an alternative system, tests have been carried out by generating an experimental result vector of coincidences $\vec{k}$ by computer and introducing statistical fluctuations. It has been assumed that all pixels contain an equal amount of activity and a number N has been defined as the number of coincidence counts emitted by each pixel into a pair of perfect opposing detectors, for $\theta = 0$. The total number of counts in one image is $N \times n^2 \times N_\theta$, with equal count density between the different tests. Fig. 6 a) shows the reconstructed 5 x 5 flat field for $N = 10^5$, $N_\theta = 16$ and Fig. 5 b) shows the results for the same N, for the 8 x 8 case, $N_\theta = 40$. Strong effects due to the eigenvector of Fig. 4 f) are quite evident in the latter. When filtering is carried out by the noise reducing pseudo-inverse of Fig. 5 b) , a substantial reduction of noise is obtained, as shown in Fig. 6 c).

Figure 7 shows the values of fractional RMS noise (n_{RMS}) obtained with the 5 x 5 and 8 x 8 systems at different values of N. A least-squares fit established quite well the relationship

$$n_{RMS} \propto (N)^{-1/2} \tag{13}$$

as expected. The numerators of the expressions shown in Fig. 7 can be defined as the corresponding relative Noise Magnification Factors (NMF) for the definition of N given above in the present case with equal counts for pixel and equal density. If we consider that the NMF could be expected to be approximately proportional to $(N_\theta)^{-1/2}$, then the dependence on CN appears to be somewhat slower than $(CN)^{1/2}$ in the region of small n explored.

Simple Imaging Experiments

In order to demonstrate the correctness of the pseudo-inverse obtained above, an imaging simulation has been carried out by generating the experimental results vector $\vec{k}$ corresponding to an n x n pixel array in which a central square portion has been given a number N, and one single pixel has 2N. Figure 8 a) shows the reconstructed image for n = 8, $N \to \infty$. Slight errors ($\simeq \pm 1\%$) occurs in three of the pixels adjacent to the 2N pixel. Errors in all the other pixels are less than $\pm$ 0.1 %. When a pseudo-inverse obtained with a 48-bit mantissa was used, the errors in the three worse pixels became approximately $\pm$ 0.8 %.

Figure 8 b) is the result of introducing fluctuations corresponding to $N = 10^5$ counts into vector $\vec{k}$, and Fig. 8 c) corresponds to the same value of N, but using the noise reducing matrix of Fig. 5 b). Such matrix reduced the noise quite strongly, as seen in Fig. 6 c), but results in very inaccurate imaging. The errors could be described as a reduction in sharpness.

Figure 8 d) shows an attempt to reconstruct an image similar to the previous ones with the "pseudo-inverse" obtained from the 27-bit mantissa QL algorithm, for n = 13. No statistical fluctuations were incorporated into vector $\vec{k}$. As indicated above, the n = 13 case could not be solved correctly with, at least, a reasonable amount of effort.

An Alternative Detector Configuration

An observation of the blurring matrices for the PET configuration described and a consideration of the fact that matrices with high condition numbers arise when the detector configuration is such that individual pixels are defined

ambiguously[2] leads to the realization that the problem of imaging a single plane activity, in the absence of activity in over or underlying planes, could best be carried out in a detector configuration which does not require the γ-ray pairs from one pixel to traverse other pixels before reaching the detectors. This can best be done by planes of detectors which are coplanar with the pixel array, a geometrical configuration that has been in use since Anger described the use of two γ-cameras for imaging positron emitting isotopes[9] in 1966. Burnham and Brownell presented their multicrystal two-plane camera for the same purpose[10] in 1972 and the concept of the planar camera configuration for three-dimensional volume reconstruction was presented by Chang et al[11] in 1976. The analysis of the problem of imaging of a single plane of activity exploiting some of the advantages of the situation by eigenanalysis has, however, not been reported in the literature and it will be the object of the following discussion.

The problem to be analyzed here is described in Fig. 9. We consider two planes with ND perfect detectors separated by a distance Z. The detector sides have dimension d. Equidistant between the two planes is an n x n array of pixels of side dimension s, where s can be smaller than d, and n^2 can be larger than ND. It will be first assumed that the centers of the pixel array and of the detector planes are colinear.

For such an imaging system the backprojection matrix A can be obtained just as in the PET case by assuming a unity of activity placed in pixel No. 1, and forming a column vector of length ND^2 containing rates of coincidences of every detector A with all detectors B for that pixel. The procedure is repeated for all n^2 pixels. Matrix A will have ND^2 rows and n^2 columns.

No restriction has been placed on which coincidences are allowed between the A and B detectors, since we are interested in maximum sensitivity by not preserving space invariance of the point response function.

The blurring matrix $A = A^T A$ for these systems presents a very different appearance from those for the PET case. Four cases have been studied, all with ND = 64 (8 x 8 detector planes), d = 1, and an increasing number of pixels of decreasing size occupying a square of sides 6 units. Table I shows the characteristics of the pixel arrays and the condition number of the blurring matrices for the planar cameras. Fig 10 a) and b) shows the blurring matrices for the n = 8 and 12 systems. The case for n = 12 corresponds to the limit imposed by sampling and finite pixel size, in which the blurring matrix becomes quite ill-conditioned, with a high CN. Figures 11 a) and b) show the blurring functions of a pixel near the center of the array for the n = 8 and 12 cases. It is evident that blurring is considerably more localized in the planar case than in the PET camera even for s = d/2.

The blurring matrices obtained for the planar cameras have been found to be exactly separable into Dirac products of X and Y blurring submatrices in the following cases tested: square detectors (as in Fig. 9), circular detectors inscribed in the squares of Fig. 9, pixel arrays which are equidistant from the two detector planes but with centers not colinear with the detector array centers, and pixels with their activity concentrated at their center. The blurring matrix is not separable in some cases tested in which the detector arrays do not appear identical under 90° rotation about the axis joining the planes. Thus, although far from exhaustive, the tests seem to indicate that uniform arrangements of detectors with substantial symmetries will result in separable matrices, which for large arrays can make the solution of the imaging problem much easier.

For the small systems tested, finding the pseudo-inverse by the method of Eq. (9) has presented no problems. The pseudo-inverse for the n = 8 and 12 cases are shown in Figs. 12 a) and b). The deblurring functions for the same two pixels of Figs. 11 a) and b) are shown in Figs. 13 a) and b). The case for n = 12, at the sampling theorem limit, requires the manipulation of the backprojected data for all the pixels in order to find the activity at on pixel, with relatively large coefficients. For s > d/2 the deblurring functions behave more like the well known functions for tomography.

The noise propagation of the planar camera with a single plane of activity has been investigated in a similar manner to the PET case. A number N has been defined as the number of counts emitted by one pixel into one pair of opposing perfect detectors. Pixels towards the center of the array contribute more counts to the image than pixels in the periphery. Figures 14 a) through c) shows the flat field images for n = 8, 10 and 12 with N = 1000. The cases for n = 8 and 10 are similar in behavior, but at the sampling theory limit, noise increases substantially.

Figure 7 shows the fractional RMS noise of the planar camera for n = 6, 8 10 and 12, obtained for the flat fields as a function of count density (Nd^2/s^2). Decreasing the pixel size from the dimension of the detector d to 0.6d would be expected to result in an increase in rms noise of 1.66 due to the decrease in counts for pixel. Since the ratio of n_{rms} is found to be 3.48, one can attribute a NMF of 2.08 to an increase in CN of 3.06. An approximate dependence of NMF $\alpha(CM)^{1/2}$ seems to hold, at least before the limit imposed by the sampling theorem is reached.

Simple imaging experiments are shown in Fig. 15. A square region of N counts per pixel per detector pair contains one pixel with 2N counts. Figure 15 a) shows an image for n = 8 comparable to the PET image of Fig. 8 b)

but N reduced by a factor of 10^3, with a similar noise level, as expected from Fig. 7. Figures 15 b) and c) show similar images for n = 10, near the sampling limit, for N = 10,000 and 10. The total number of counts in the image for n = 10 is approximately 10,000. Finally, Fig. 15 d) shows the n = 12 image for N = 10 with considerable deterioration over the one of Fig. 15 c).

Regarding the method of solution, it can be indicated that the well behaved matrices of the planar camera, except for the n = 12 case, correspond to problems which can be solved with quite satisfactory results by several methods: pseudo-inverse (Eqs. 8 and 9), separated X and Y pseudo-inverse (Eqs. 11 and 12), direct solution of Eq. (3) by inversion of A', and a linear least squares solution with non-negative constrain on the result.[12] There are some differences in the solutions with noisy data, but they are minor. The method of choice may depend on the specific application.

Inclusion of TOF Information in PET

The first part of this paper has demonstrated without much doubt that the problem of image reconstruction from a section using transverse tomography by an exact approach (as exact as the model used to describe the imaging system by the backprojection matrix) is not practical except for very small systems. This result is not new, as that approach has not had much appeal for workers in the tomographic imaging field. The detailed examination carried out, however, has given a good indication of the reason for the difficulty and pointed out that, at least in some specific cases, there may be alternatives

to a detector ring structure which have very desirable noise behavior and ease of solution, even with large arrays.

A comparison between the calculations for the PET and planar structures shows that the very high CNs of the PET matrices are caused by the large amount of ambiguity about the origin of a γ-ray pair when the rays have to cross many pixels before reaching the detectors. In single plane imaging with planar cameras the knowledge of the point of origin along the trajectory of the γ-ray pair is implicitly included in the A matrix so that the deblurring process only has to contend with the effects of nearest neighbor pixels.

An immediate corollary that comes out from the above discussion is that the newly emerging time-of-flight (TOF) technology for imaging positron emitters can contribute substantially to posing the PET imaging problem in improved terms by removing a very substantial part of the ambiguity in the matrices, although the time resolution of the TOF systems is not ideal.

In order to demonstrate this point explicitly, the simple imaging system of Fig. 1 has been reanalyzed by assuming that the detectors have TOF capability with a Gaussian space resolving function of standard deviation (σ_{TOF} x d). Each column of the system matrix A corresponding to one pixel is now expanded to contain one entry for each TOF analyzer bin for each projection bin for each projection, i.e., the length of each column of A is (N_{TOF} x N_c x N_θ), where N_{TOF} is the number of TOF bins used in the analysis. The entries in A have been filled with the values of a Gaussian function of mean equal to the mean TOF difference from the portion of pixel spanned by the corresponding detector pair and a given standard deviation σ_{TOF}. The area of the Gaussian has been made equal to the portion of pixel area spanned, i.e., the area of the Gaussian is equal to the single bin entry

without TOF information. This is a formal approach to representing the detection system, since each column entry is one possible outcome of the measurement and the entry values are probabilities of such outcome being true.

The A-matrix thus obtained can then be used to obtain the blurring and deblurring matrices for the system, as described above. Results for an 8 x 8 pixel array, $N_\theta = 32$ and σ_{TOF} ranging between 0.75d to 4.5d have been obtained and are shown in Table II. The fractional RMS noise corresponds to a flat field with a number N of counts emitted by one pixel into one pair of opposing detectors equal to 1000. The strong improvement in CN of the blurring matrices with improving σ_{TOF} is very evident. The RMS noise is found to follow approximately the relationship

$$n_{RMS} \quad \alpha(CN)^{.37} \tag{14}$$

for $\sigma_{TOF} = 4.5d$ and below. The RMS noise follows a nearly linear relationship with σ_{TOF} for values of the latter between 3.0d and 0.75d.

The effect of including TOF information on the character of the blurring matrices is quite evident from Fig. 16 a) through c) showing the blurring functions for the first pixel of the 8 x 8 array for the case of no TOF, and $\sigma_{TOF} = 4.5d$ and 1.5d. Figures 17 a) through c) show the corresponding deblurring functions. The sharpening of the blurring functions with improved TOF information leads to a "cleaning up" of the deblurring functions which are seen to approach the customary filter functions of computed tomography in appearance.

Conclusion

The above matrix analysis of the transverse tomography problem has shown that considerable insight can be gained on the reasons for its ill-posed nature, which prevents an exact solution of practical medical cases. The inclusion of TOF information makes a very substantial difference on the conditions of the problem, even with time resolutions which corresponds to a determination of the point of γ-ray emission with uncertainities of several times the pixel dimensions. The inclusion of the TOF information into the system matrix has been seen to lead to the determination of filter functions which are specific to a particular detector system. Carrying the idea to the extreme of exact TOF knowledge by postulating that the positron emitting activity is all in one single plane and designing a planar camera to take advantage of that fact results in a detector system with excellent condition in which the solution can be pushed to cases with pixel size smaller than the detector size.

The detector systems simulated in the present work have been assumed to be perfect. A physical system will have a number of imperfect features which will result in blurring matrices of somewhat worse characteristics than the ones shown here. Previous experience with a one-dimensional camera[3] shows that the CN of a physical detector system can be larger by a factor of roughly two when compared to a calculated model. For the case of radioactive beam injection[1], the design of a high sensitivity and high spatial accuracy two-dimensional instrument for single plane imaging is proceeding following the above concepts of a planar camera. A computer camera simulation program, including neighboring detector interactions, is going to be used in the design process and to obtain the filter functions for the actual instrument.

It is expected that true three-dimensional imaging (activity in a volume, rather than a plane) by the pseudo-inverse method demonstrated in this paper will run immediately into similar ambiguity problems as the PET problem. There is, however, a large number of ideas to be explored regarding detector configuration, separability of the matrices and TOF before a reasonably complete understanding of the role of eigenanalysis techniques in three-dimensional image reconstruction is attained. This work will proceed a part of our radioactive beam project at LBL.

Acknowledgement

The author would like to thank A. Chatterjee, E.L. Alpen, and F.S. Goulding for their support, encouragement and discussions during the course of this work, and M. Ter-Pogossian for asking some incisive questions which, hopefully, have been answered in this paper.

Figure Captions

1. Simple PET camera model for matrix analysis. An n x n array of square pixels p of dimension d is looked at by two banks (a and b) of perfect γ-ray detectors, each with N_c detectors, which rotate over an angle θ. Coincidences are only allowed between exactly opposing pairs of detectors. Their response to a pixel of uniform activity is proportional to the pixel area (shaded) spanned by the detector.

2. Blurring matrix for an 8 x 8 pixel array. Matrix dimension is 64 x 64. Each column (or row) contains all the blurring information for one pixel. A very high condition number (CN) is shown for this matrix.

3. Blurring function for a corner pixel of the 8 x 8 array. It corresponds to the first column of the matrix of Fig. 2, plotted on an 8 x 8 array. The values of the function corresponds to the image that would be obtained from a single active pixel if only backprojection of the coincidence data were carried out (no filtering).

4. Some eigenvectors of the blurring matrix of Fig. 2.
   a), b) and c): Lowest spatial frequency eigenvectors, corresponding to the largest eigenvalues.
   d), e) and f): Eigenvectors with smallest eigenvalues, which have deviated from a resemblance to two-dimensional sinusoidal function products.

5. Pseudo-inverse matrix for the 64 x 64 matrix of Fig. 2.
   a) Unmodified, matrix is dominated by some large positive and negative elements, which obscure structure in all columns.
   b) Modified by exclusion of terms corresponding to smallest eigenvalues. The elements with very large magnitude have disappeared.

6. Response of the PET system to a flat field of activity. The number of counts N emitted by each pixel into an opposing pair of detectors for each angle measured is 100,000.
   a) 5 x 5 pixel array
   b) 8 x 8 pixel array
   c) 8 x 8 pixel array, using modified pseudo-inverse of Fig. 5 b)

7. Fractional rms noise (rms noise activity/activity) as a function of count density for flat field PET images with n = 5 and 8. Also for planar camera with n = 6, 8, 10 and 12. Solid lines are fitted to computer simulation points showing $n_{RMS} \propto N^{-1/2}$.

8. Simple imaging simulation experiments for the 8 x 8 pixel PET system. A 4 x 4 square of unit activity contained one pixel of two units activity.
   a) No statistical fluctuations in the data. Notice small errors adjacent to the two unit pixel caused by truncation errors in the pseudo-inverse.
   b) With statistical fluctuations corresponding to N = 100,000.
   c) N = 100,000, filtering done with noise-reducing matrix of Fig. 5 b).
   d) Similar experiment with 13 x 13 pixel PET system, no statistical fluctuations, showing considerable errors caused by faulty inverse.

9. Schematic drawing of planar camera for single plane image reconstruction from an accelerated radioactive ion beam injection. Two banks of square perfect detectors (A and B) of dimension d are equidistant from a plane of n x n square pixels of dimension s, where s d. Each pixel is assumed to contain a uniform activity. All possible coincidences are allowed between the two banks of detectors.

10. Blurring matrices for planar camera with 8 x 8 detectors of dimension d.
    a) For 8 x 8 pixel array (n = 8) of dimension s = 0.75d.
    b) For 12 x 12 pixel array (n = 12) of dimension s = 0.5d (sampling limit).

11. Blurring functions for a pixel near the center of the array (columns of the matrices of Fig. 10).
    a) n = 8
    b) n = 12

12. Pseudo-inverses for the matrices of Fig. 10.
    a) n = 8
    b) n = 12

13. Deblurring functions for a pixel near the center of the array (columns of the matrices of Fig. 12).
    a) n = 8
    b) b = 12

14. Response of the planar detector system of Fig. 9 to a flat field of activity. The number of counts N emitted by each pixel into any opposing pair of detectors is 1000. Compared with Fig. 6 b) it is seen that similar noise levels are obtained in the planar camera with 100 times fewer counts, with value of s up to very close to the sampling limit.

    a) For n = 8, s = 0.75d

    b) For n = 10, s = 0.6d

    c) For n = 12, s = 0.5d (sampling limit)

15. Simple imaging experiments for the 8 x 8 planar detector system, similar to those of Fig. 8.

    a) n = 8, N = 100

    b) n = 10, N = 10,000

    c) n = 10, N = 10. Notice that image is still quite good, even at s = 0.6d and with few counts.

    d) n = 12, N = 10. Large errors occur at the sampling limit with poor statistics.

16. Blurring functions for 8 x 8 system of Fig. 1 with inclusion of TOF information. System is almost identical ($N_\theta = 32$ instead of 40) to that of Fig. 3.

    a) No TOF information

    b) with $\sigma_{TOF} = 4.5d$

    c) with $\sigma_{TOF} = 1.5d$

17. Deblurring functions corresponding to the same system and pixel of Fig. 16.

    a) no TOF information

    b) with $\sigma_{TOF} = 4.5d$

    c) with $\sigma_{TOF} = 1.5d$

References

1. A. Chatterjee, E.L. Alpen, C.A. Tobias, J. Llacer and J. Alonso. "High Energy Beams of Radioactive Nuclei and Their Biomedical Applications". Int. Journal Radiation Oncology Biol. Phys., Vol. 7, pp. 503-507, 1981.

2. J. Llacer, "Theory of Imaging with a Very Limited Number of Projections". IEEE Trans. Nuclear Science, NS 26, No. 1, 1979.

3. J. Llacer, A. Chatterjee, B. Jackson, J. Lin and V. Zunzunegui, "An Imaging Instrument for Positron Emitting Heavy Ion Beam Injection". IEEE Trans. Nuclear Science, NS 26, No. 1, 1979.

4. H.C. Andrews and B.R. Hunt, "Digital Image Restoration", Prentice-Hall, 1977.

5. Z.H. Cho, "General Views of 3-D Image Reconstruction and Computerized Transverse Axial Tomography". IEEE Trans. Nuclear Science, NS 21, No. 3, pp. 44-71, June 1974.

6. Subroutine EIGEN, RT-11 FORTRAN Scientific Subroutine Package, Digital Equipment Corporation.

7. Subroutine EIGRS, Advanced Math Library, Floating Point Systems, Inc.

8. Driver Subroutine RS, Calling TRE02 and TQL2 of Library EISPACK, Argonne National Laboratory.

9. H.O. Anger, IEEE Trans. Nuclear Science, NS 13, No. 3, p. 380, 1966.

10. C.A. Burnham and G.L. Brownell, IEEE Trans. Nuclear Science, NS 19, No. 3, p. 201, 1972.

11. L.T. Chang, B. Macdonald and V. Perez-Mendez, IEEE Trans Nuclear Science, NS 23, p. 568, 1976.

12. C.L. Lawson and R.J. Hanson, "Solving Least Squares Problems". Prentice-Hall Series on Automatic Computation, Ch. 23, 1974.

TABLE 1

Condition Numbers of Blurring Matrices

System	Pixel Array n	A Matrix Dim	No. of Angles N_θ	No. of Coinc./Angle N_c	CN	Method
PET Fig. 1	5	25 x 25	8	9	14690	Jacobi 55-bit
	5	25 x 25	16	9	2463	QL 27 and
	5	25 x 25	32	9	2464	48-bit
	8	64 x 64	24	12	277440	QL 27-bit
	8	64 x 64	40	12	272500	
	8	64 x 64	40	12	271593	QL 48-bit
			Pixel Size s	No. of Coinc.		
Planar Fig. 9	6	36 x 36	1.0 d	64 x 64 = 4096	9.7	
	8	64 x 64	0.75 d	4096	16.03	QL 27-bit
	10	100 x 100	0.6 d	4096	29.7	
	12	144 x 144	0.5 d	4096	5508	

TABLE II

Effect of Including TOF Information On System Matrices

PET System of Fig. 1, n = 8, n_θ = 32, QL 27-bit Eigenvalues

σTOF	CN	Fractional RMS noise N = 1000
No TOF	305255	≃ .3
4.5 d	2498	.027
3.0 d	1023	.022
1.5 d	189.5	.0117
0.75 d	44	.0062

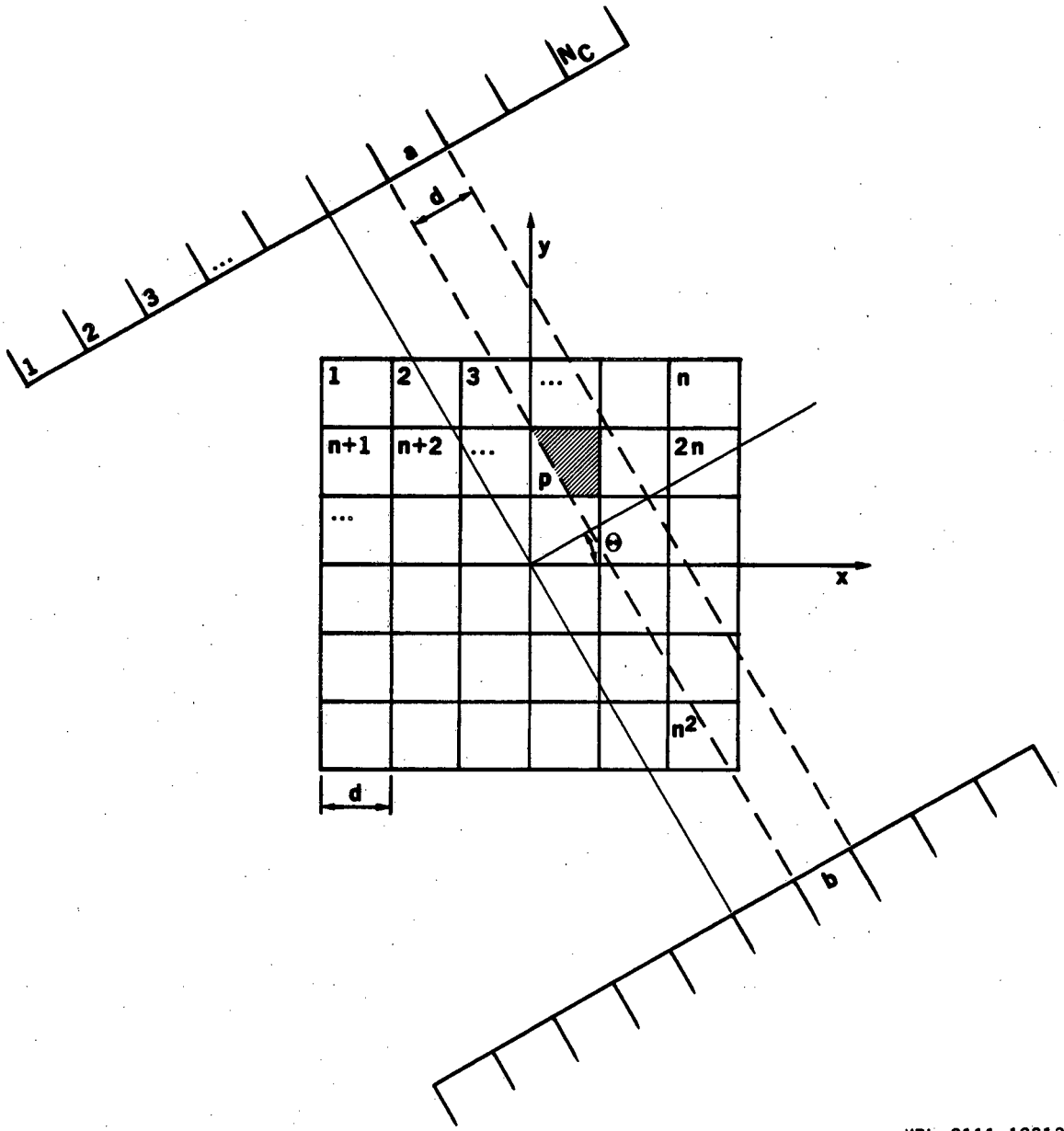

Figure 1

XBL 8111-12313

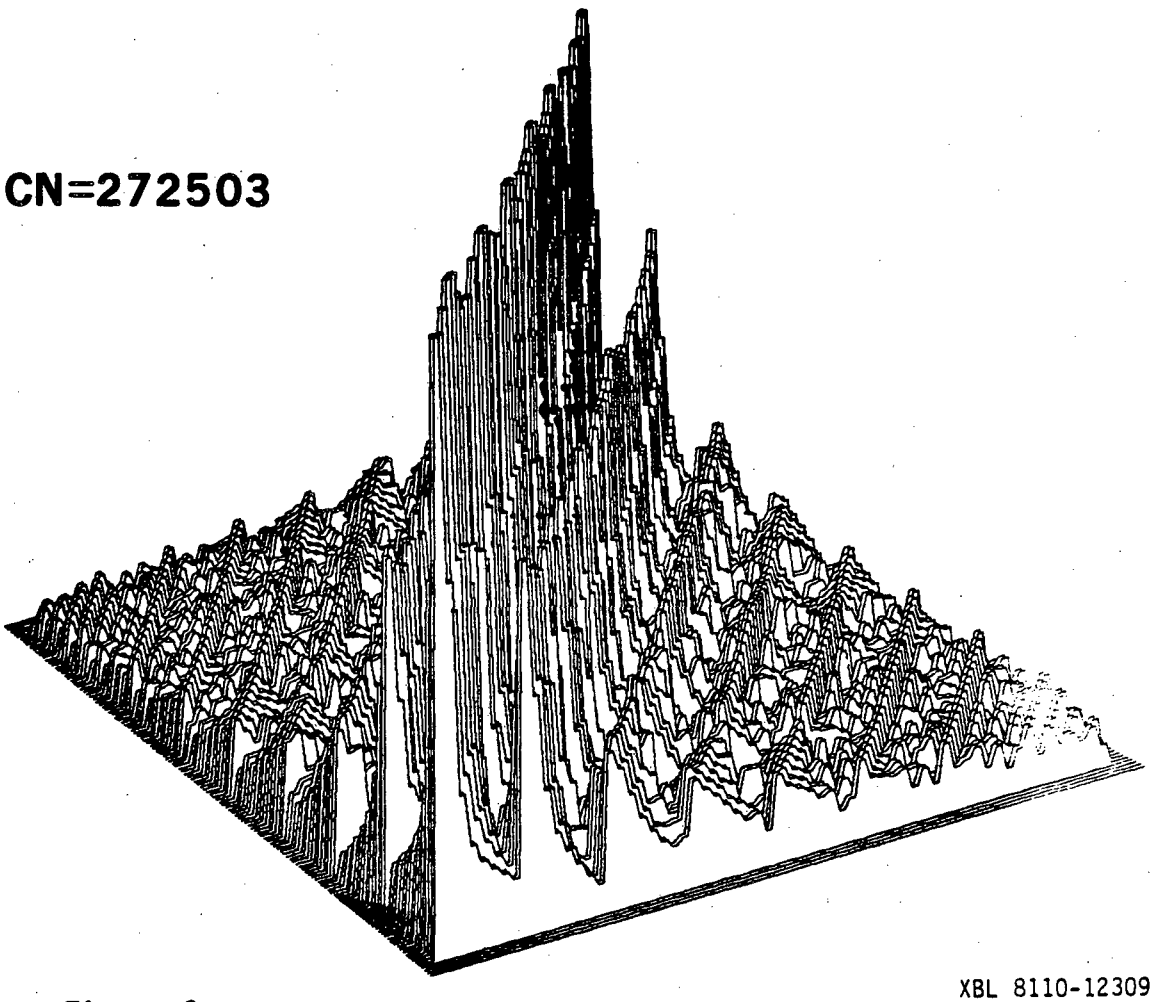

XBL 8110-12309

Figure 2

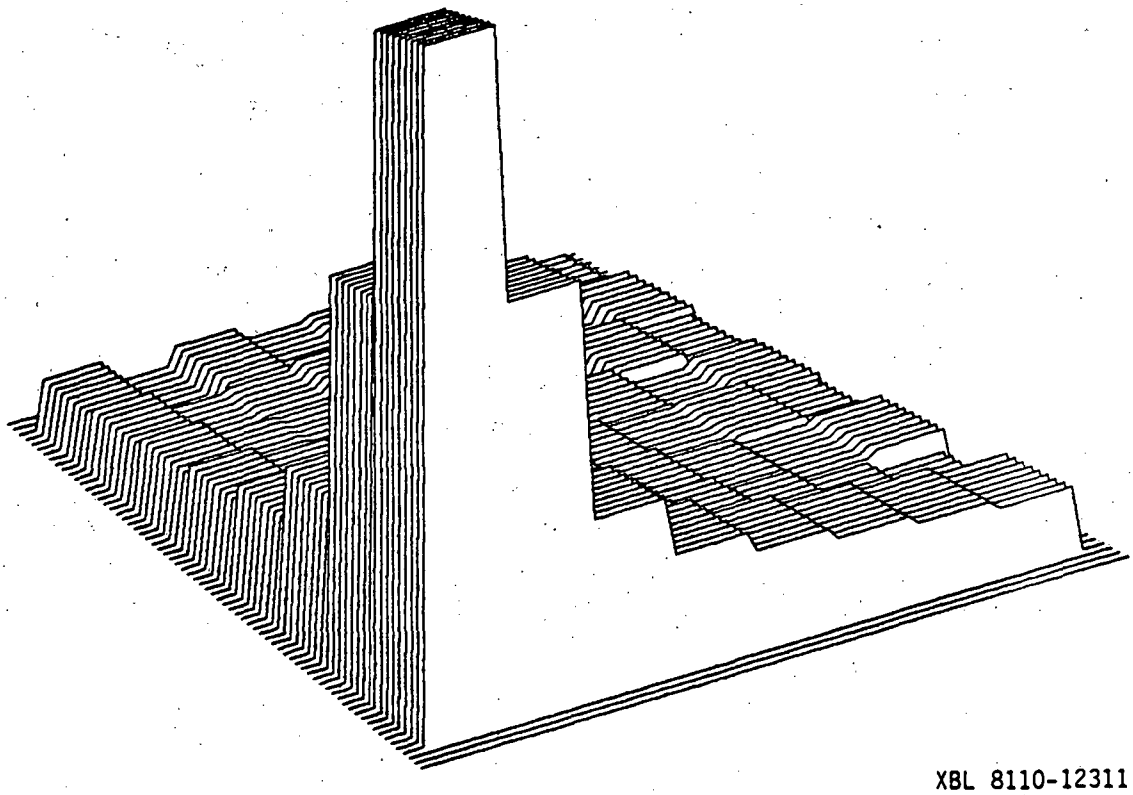

XBL 8110-12311

Figure 3

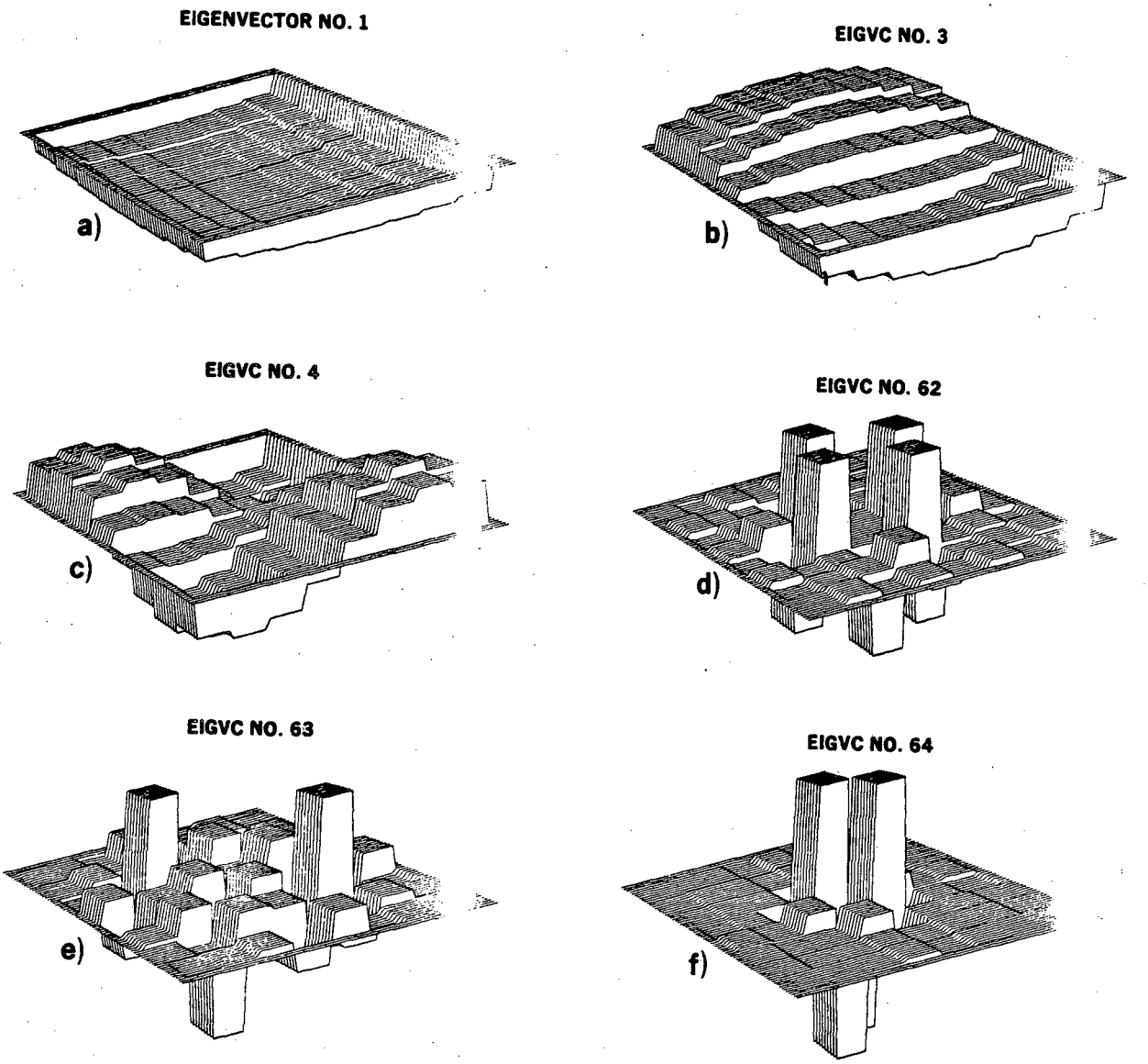

Figure 4

XBL 8110-12321

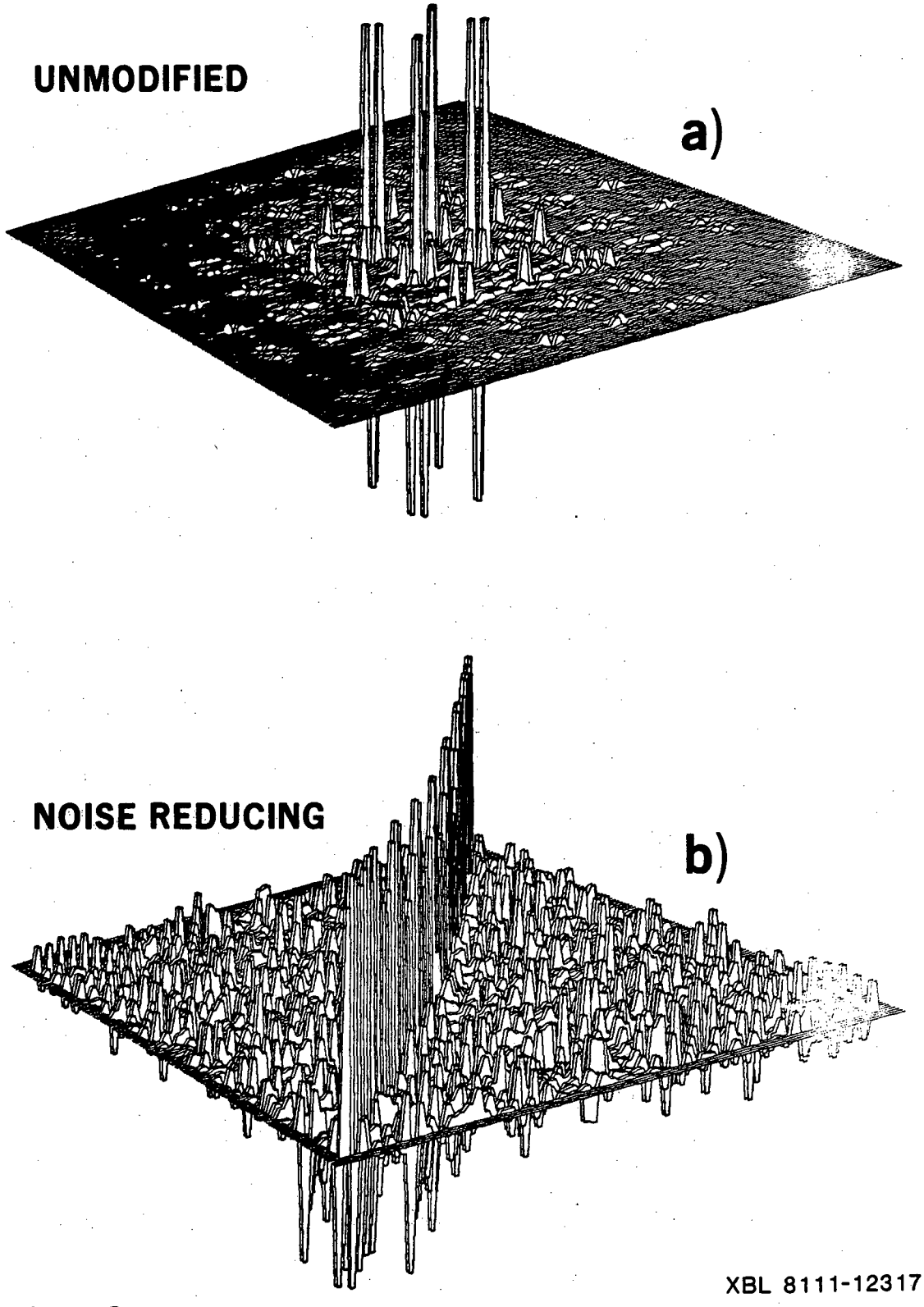

XBL 8111-12317

Figure 5

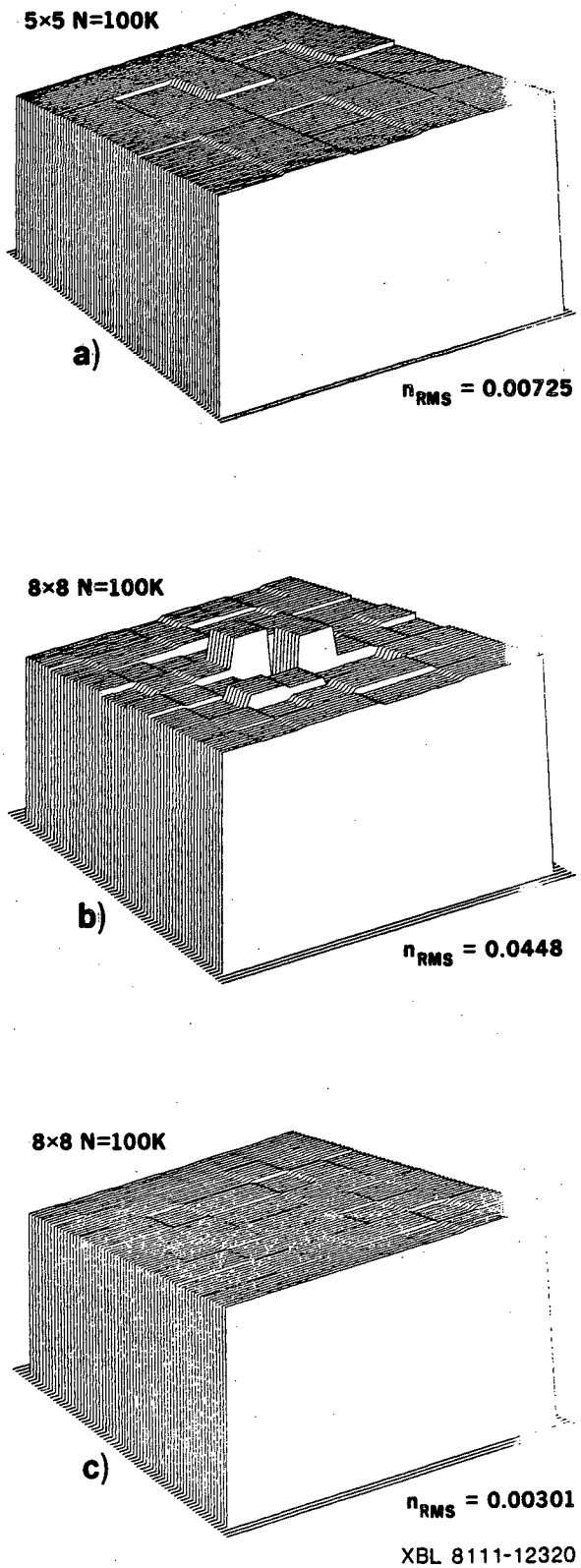

XBL 8111-12320

Figure 6

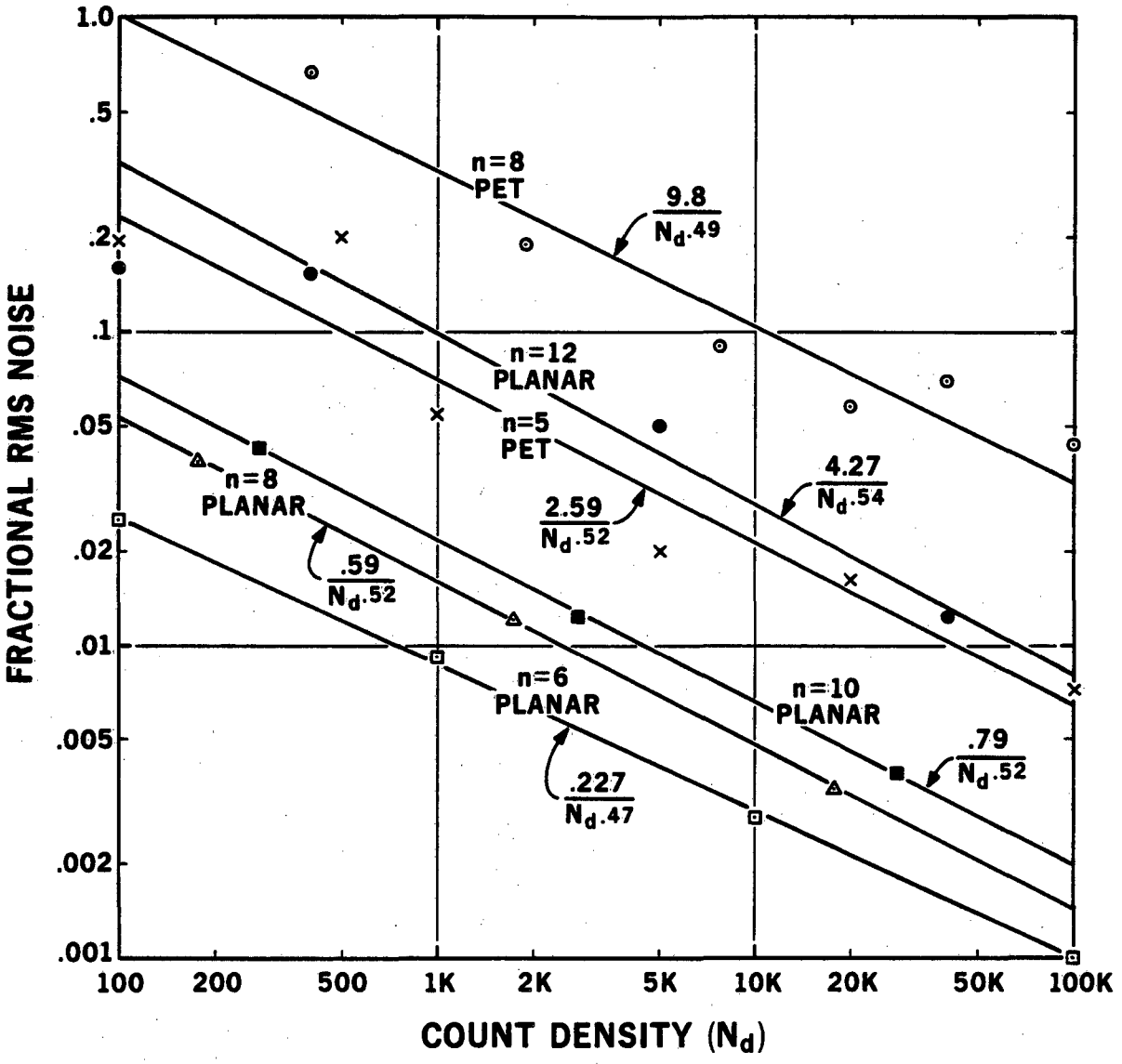

Figure 7

XBL 8111-12312

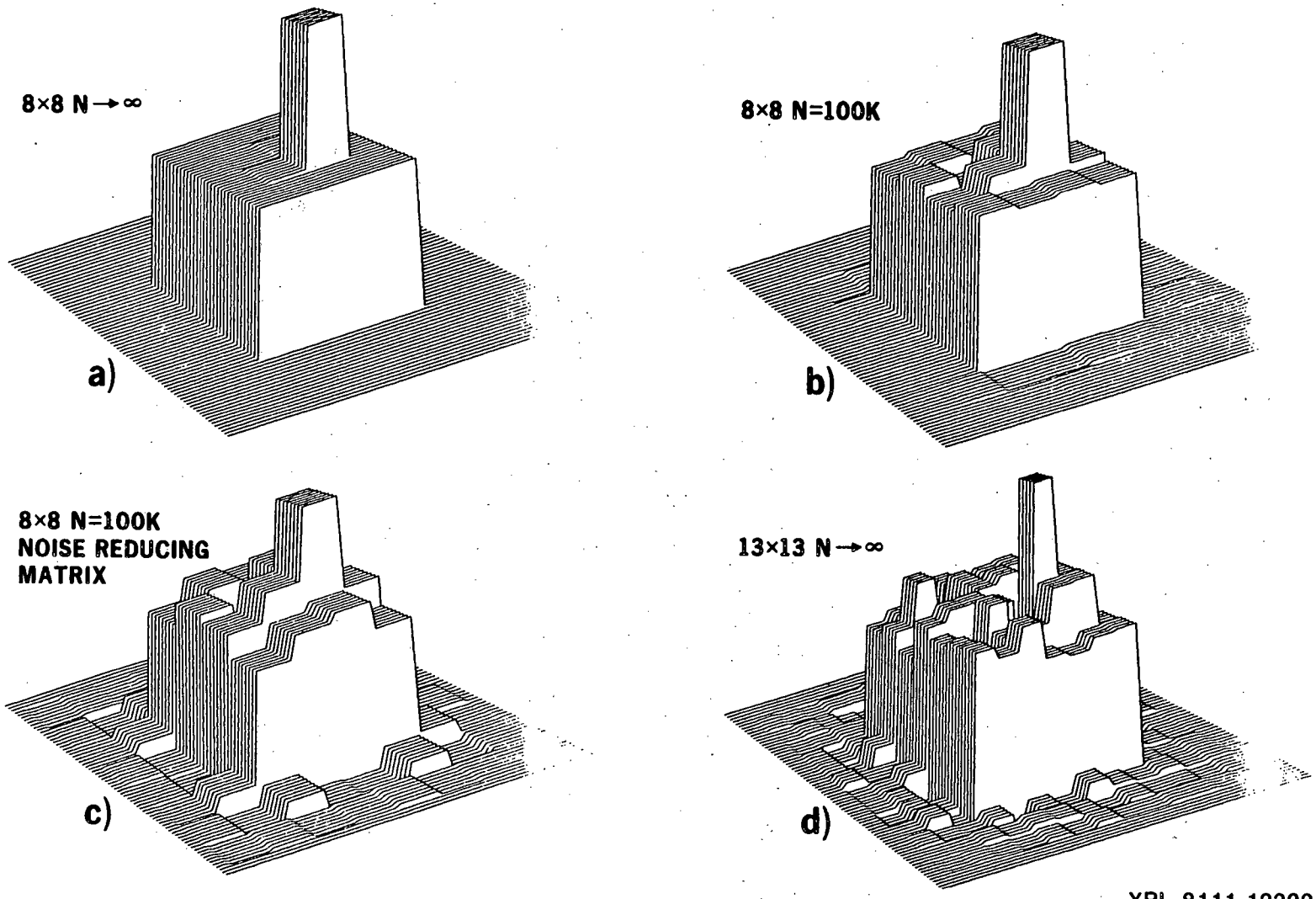

XBL 8111-12322

Figure 8

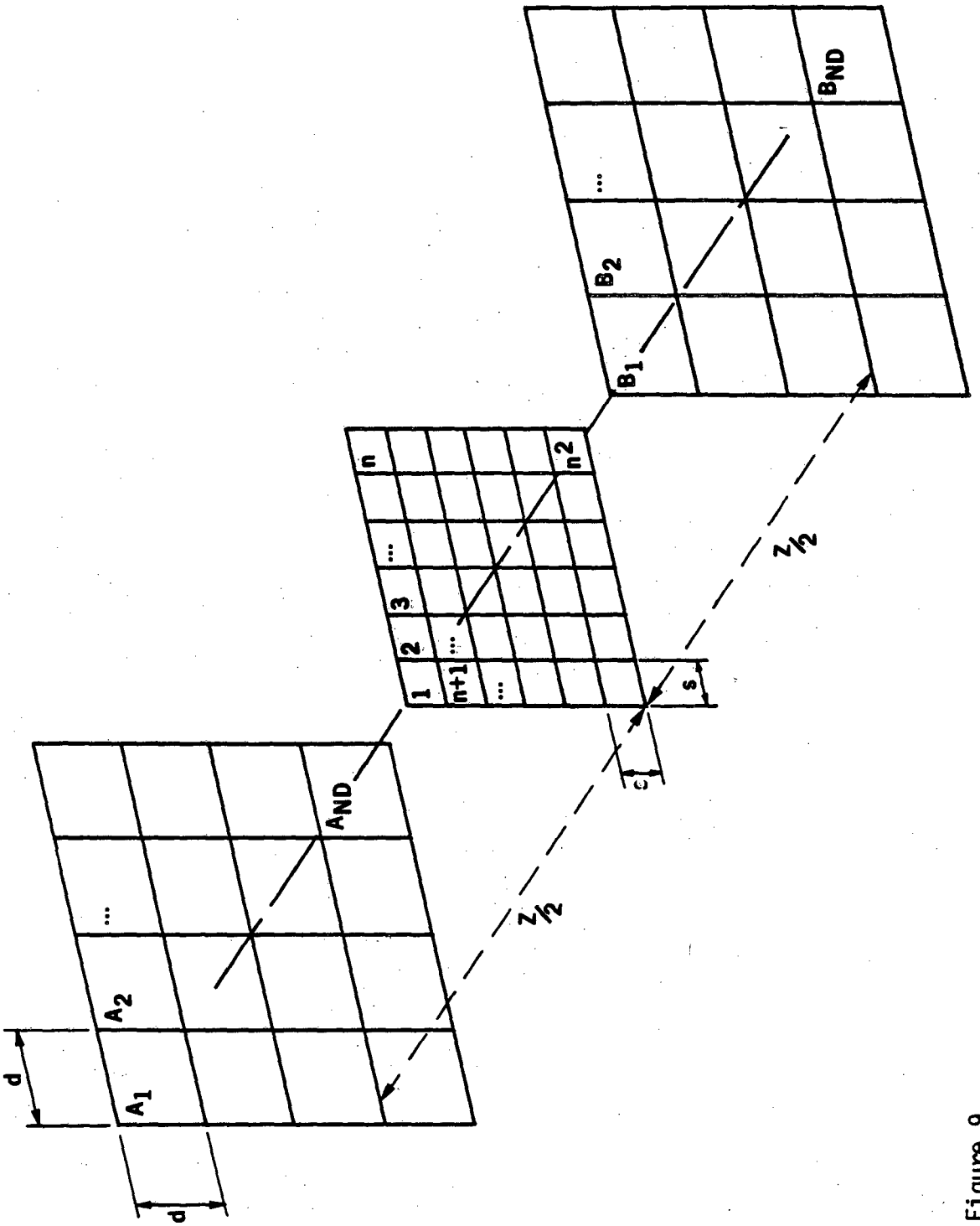

XBL 8111-12314

Figure 9

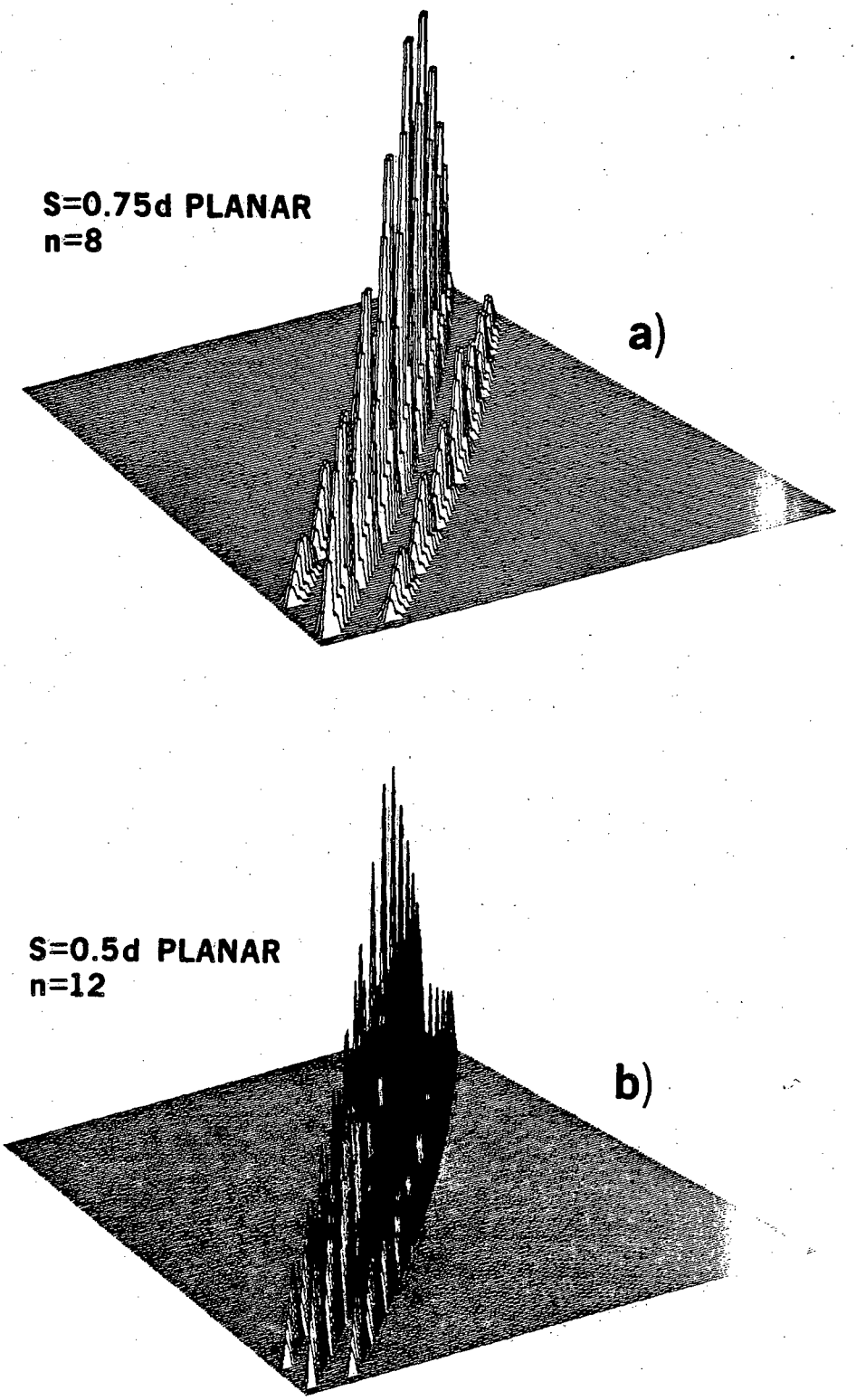

Figure 10

XBL 8111-12318

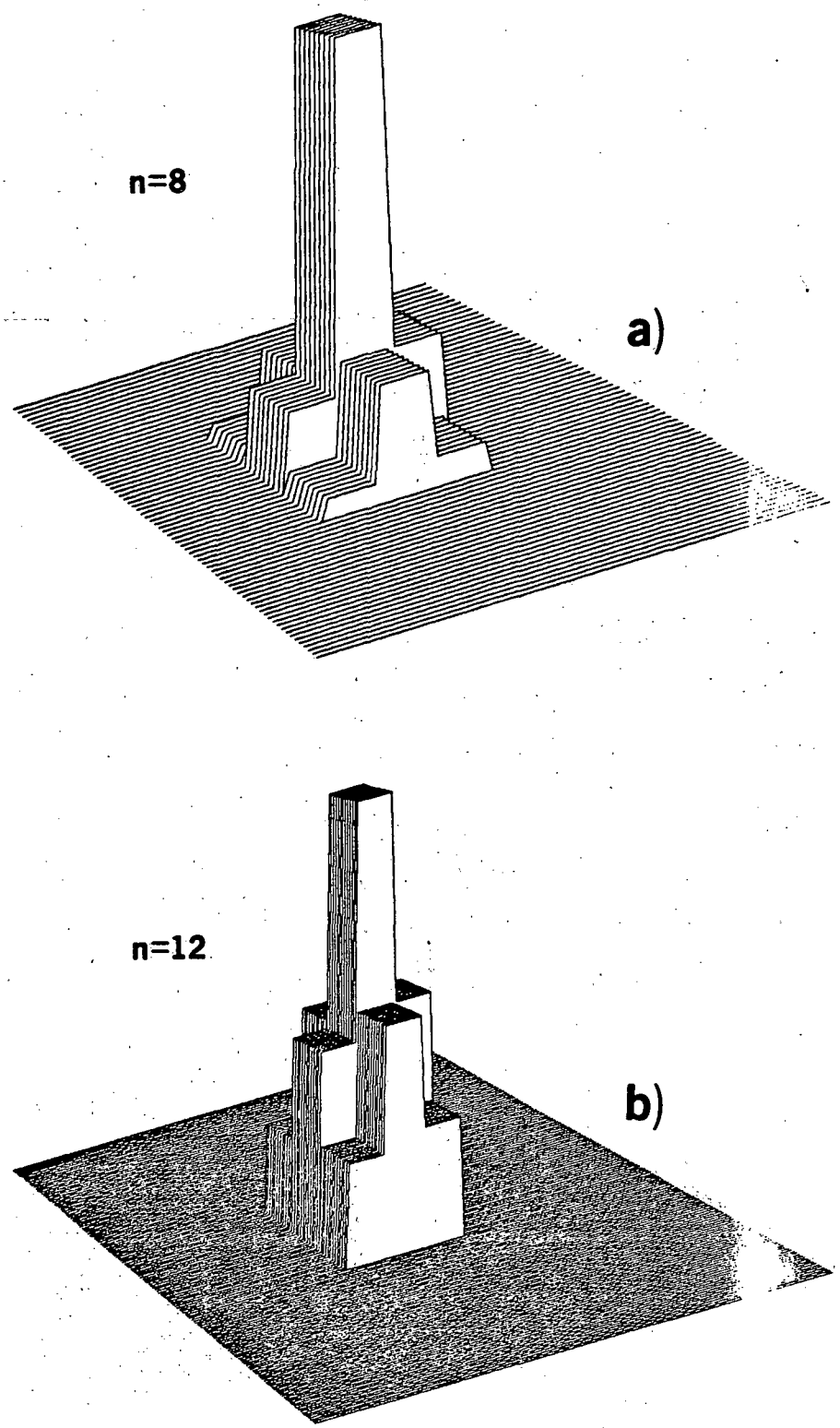

Figure 11

XBL 8111-12315

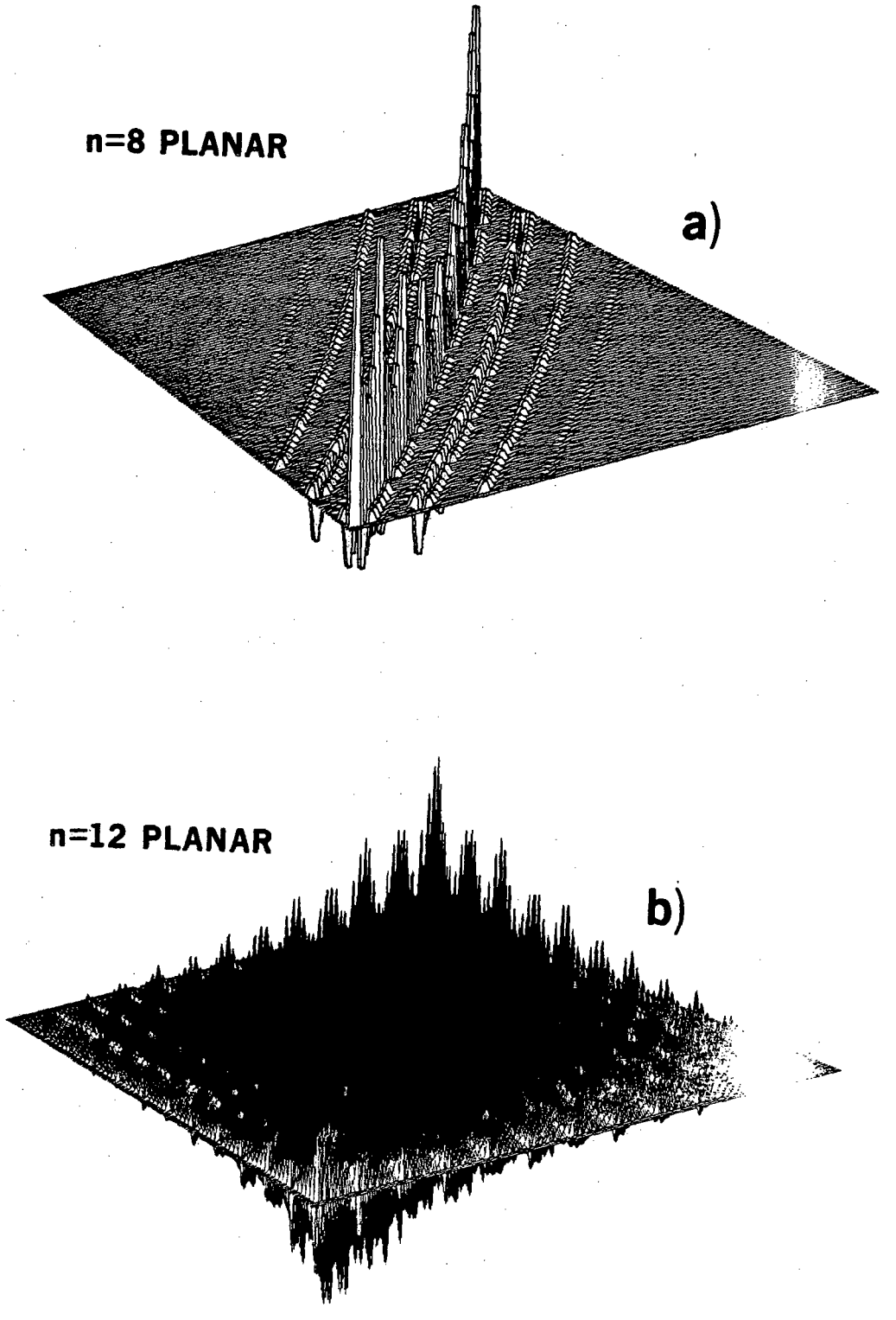

Figure 12

XBL 8111-12319

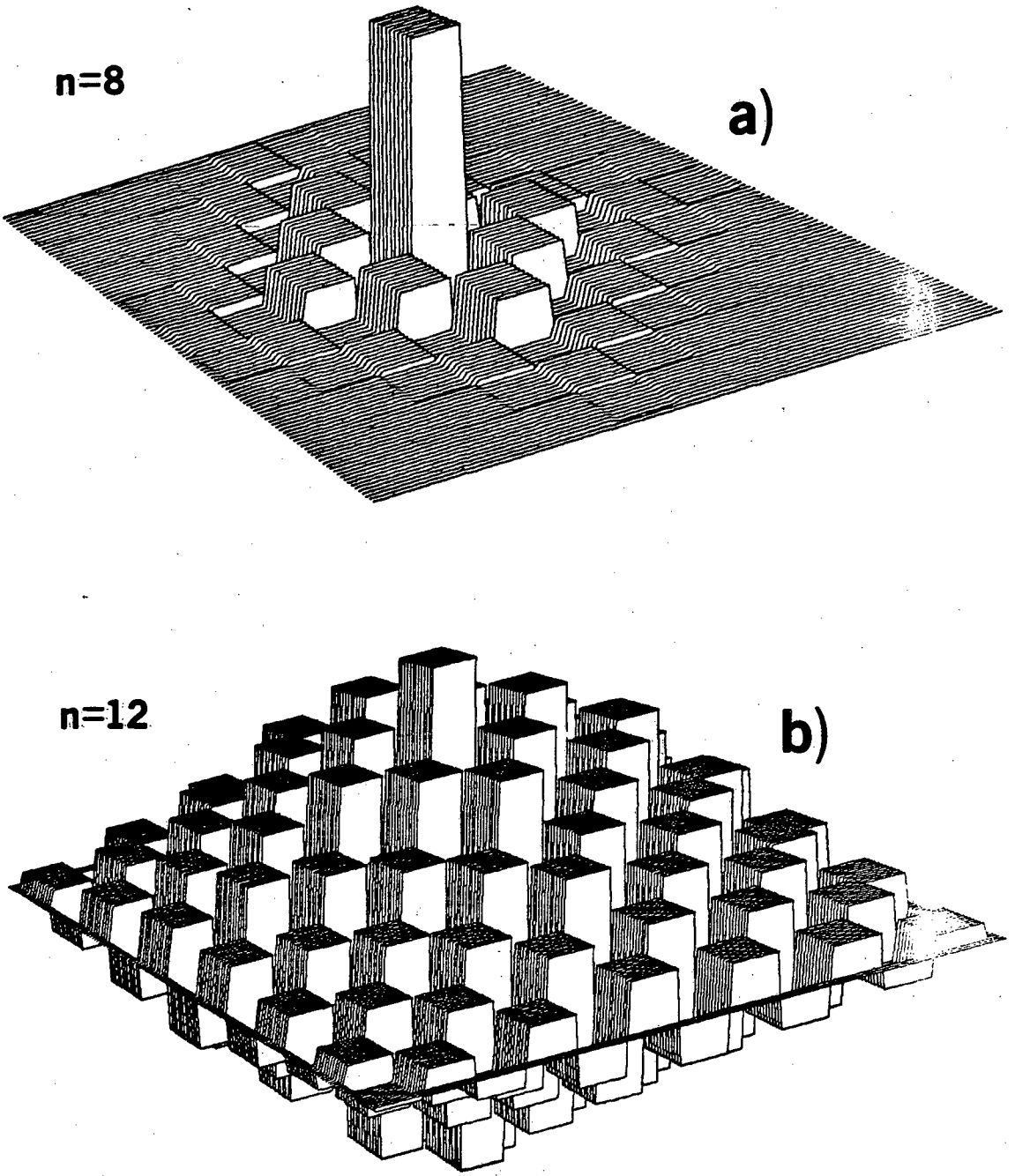

Figure 13

XBL 8111-12316

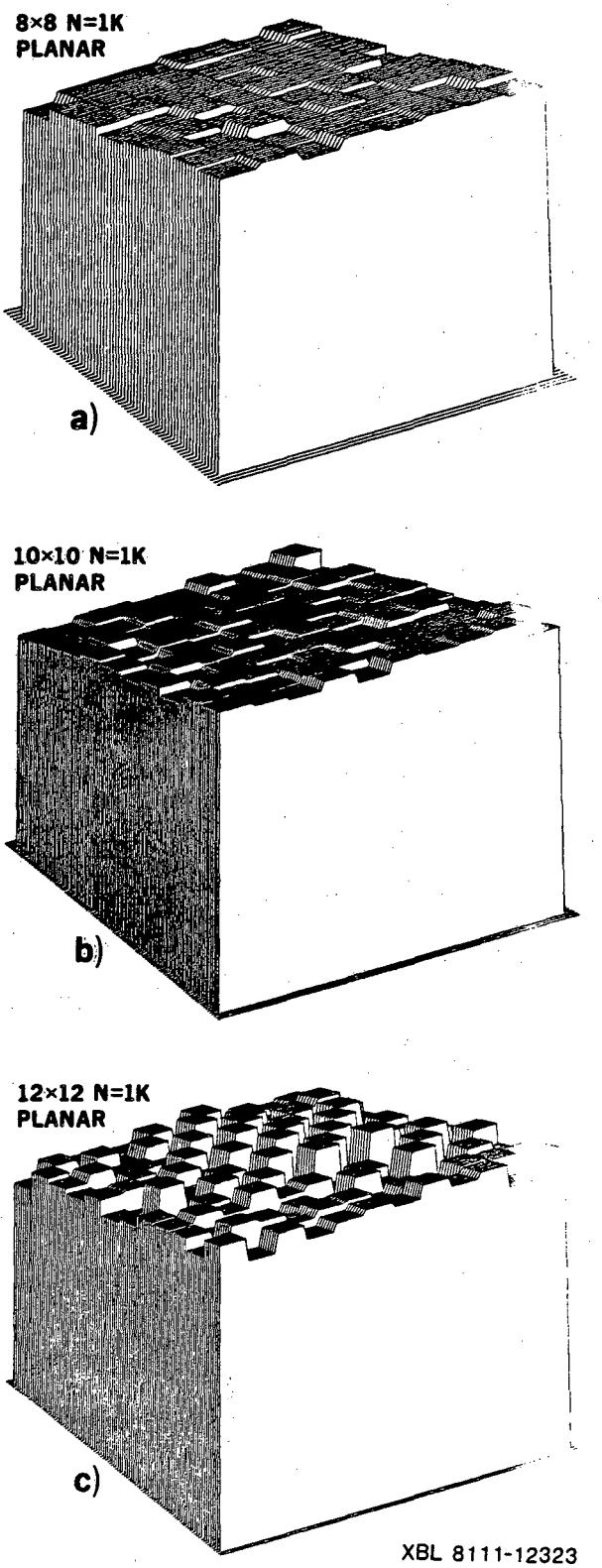

Figure 14

XBL 8111-12323

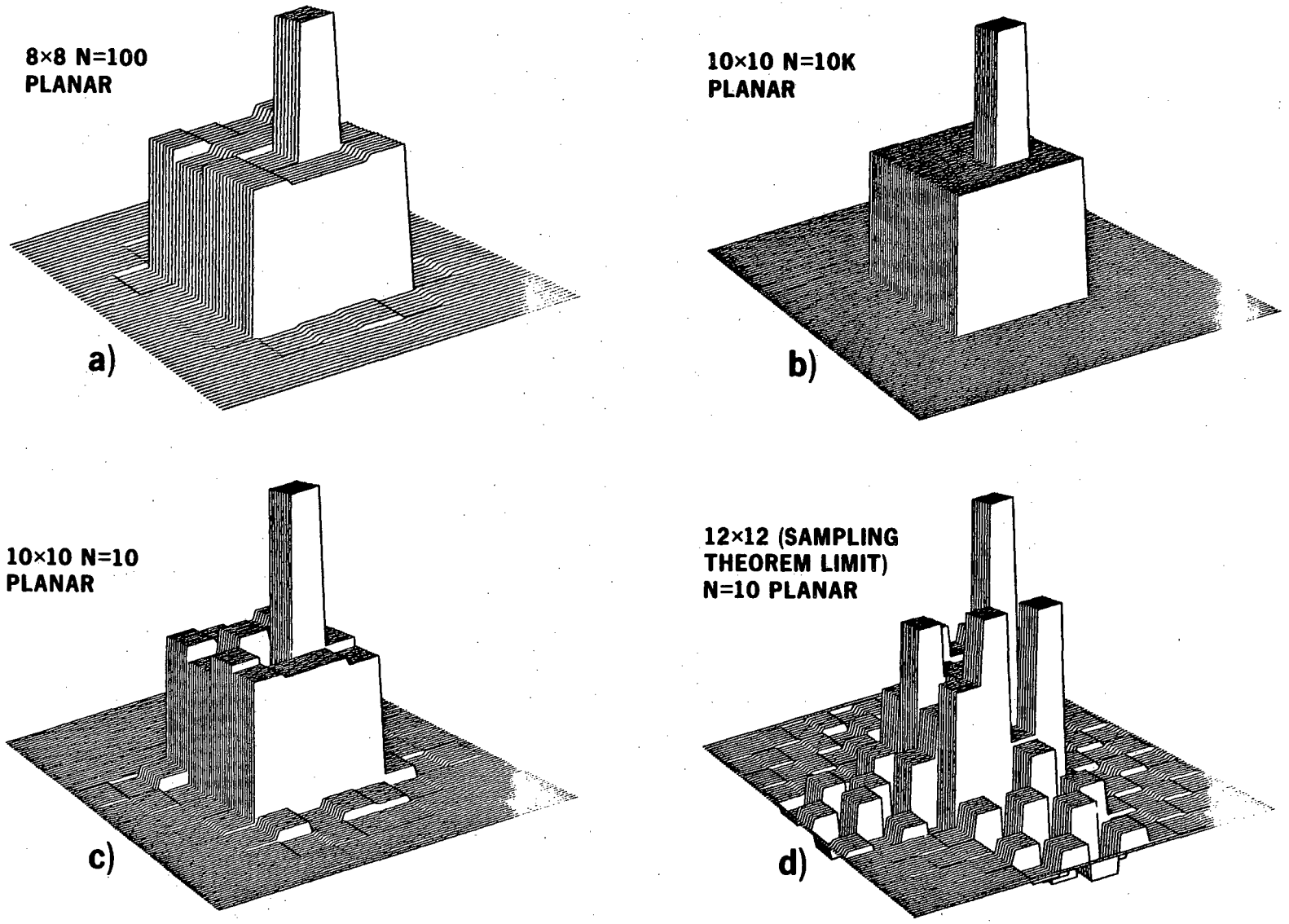

Figure 15

XBL 8111-12324

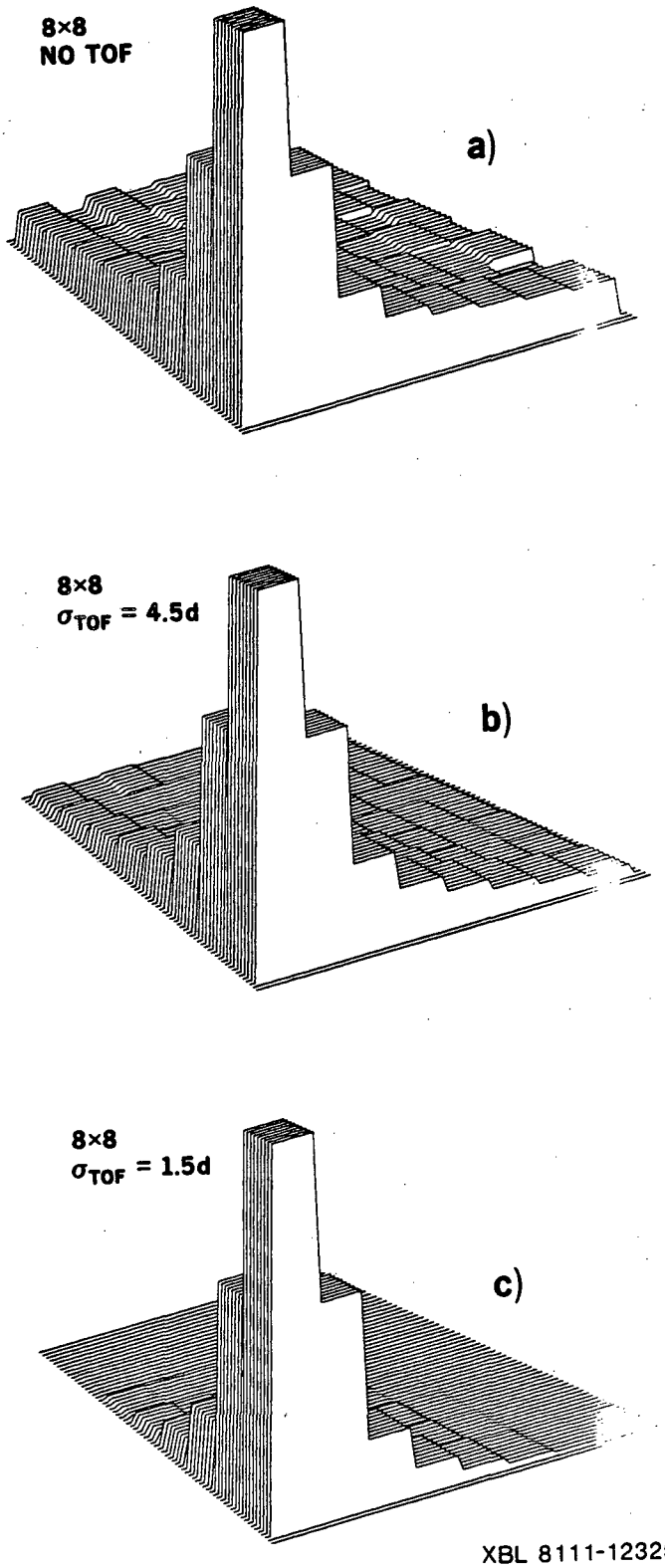

Figure 16

XBL 8111-12325

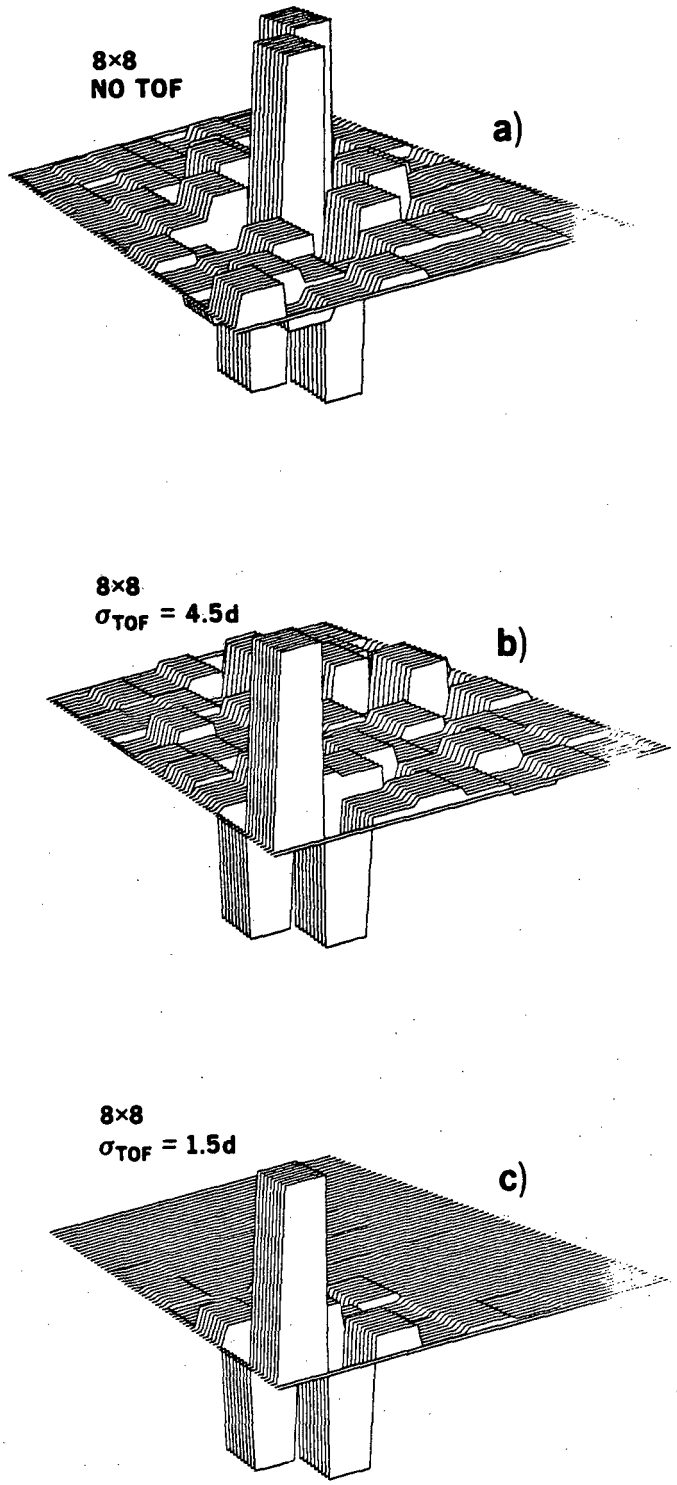

Figure 17

XBL 8111-12326

This report was done with support from the Department of Energy. Any conclusions or opinions expressed in this report represent solely those of the author(s) and not necessarily those of The Regents of the University of California, the Lawrence Berkeley Laboratory or the Department of Energy.

Reference to a company or product name does not imply approval or recommendation of the product by the University of California or the U.S. Department of Energy to the exclusion of others that may be suitable.

TECHNICAL INFORMATION DEPARTMENT
LAWRENCE BERKELEY LABORATORY
UNIVERSITY OF CALIFORNIA
BERKELEY, CALIFORNIA 94720